Manipulating magnetic and magnetoresistive properties by oxygen vacancy complexes in GCMO thin films

Beiranvand, A.; Liedke, M. O.; Haalisto, C.; Lähteenlahti, V.; Schulman, A.; Granroth, S.; Palonen, H.; Butterling, M.; Wagner, A.; Huhtinen, H.; Paturi, P.;

Originally published:

February 2022

Journal of Physics: Condensed Matter 34(2022)15, 155804

DOI: https://doi.org/10.1088/1361-648X/ac4eac

Manipulating magnetic and magnetoresistive properties by oxygen vacancy complexes in GCMO thin films

A. Beiranvand[1], M. O. Liedke[2], C. Haalisto[3], V. Lähteenlahti[1], A. Schulman[1], S. Granroth[3], H. Palonen[1], M. Butterling[2], A. Wagner[2], H. Huhtinen[1] and P. Paturi[1]

[1] Wihuri Physical Laboratory, Department of Physics and Astronomy, University of Turku, FI-20014 Turku, Finland

[2] Helmholtz-Zentrum Dresden–Rossendorf, Institute of Radiation Physics, Bautzner Landstraße 400, 01328 Dresden, Germany

[3] Laboratory of Materials Science, Department of Physics and Astronomy, University of Turku, FI-20014 Turku, Finland

E-mail: azabei@utu.fi

November 2021

Abstract. The effect of *in situ* annealing is investigated in $Gd_{0.1}Ca_{0.9}MnO_3$ (GCMO) thin films in oxygen and vacuum atmospheres. We show that the reduction of oxygen content in GCMO lattice by vacuum annealing induced more oxygen complex vacancies in both subsurface and interface regions and larger grain domains when compared with the pristine one. Consequently, the double exchange interaction is suppressed and the metallic-ferromagnetic state below Curie temperature turned into spin–glass insulating state. In contrast, the magnetic and resistivity measurements show that the oxygen treatment increases ferromagnetic phase volume, resulting in greater magnetization (M_S) and improved magnetoresistivity properties below Curie temperature by improving the double exchange interaction. The threshold field to observe the training effect is decreased in oxygen treated film. In addition, the positron annihilation spectroscopy analysis exhibits fewer open volume defects in the subsurface region for oxygen treated film when compared with the pristine sample. These results unambiguously demonstrate that the oxygen treated film with significant spin memory and greater magnetoresistance can be a potential candidate for the future memristor applications.

1. Introduction

Rare earth perovskite manganites of $RE_{1-x}A_xMnO_3$, where RE and A are trivalent lanthanide and divalent alkaline earth ions, are widely studied due to their colossal magnetoresistance, metal-insulator transition and high Curie temperature [1, 2, 3, 4]. During these years, the conducted research have pointed out that the properties of the complex perovskite manganites are mainly due to the ratio of different oxidation states

of manganese ions [5, 6, 7]. Usually, the ratio of Mn^{3+}/Mn^{4+} is tuned by substitution of RE by divalent alkaline elements [6, 8, 9]. Another way to change this ratio in thin films is controlling the oxygen content by applying partial oxygen/vacuum pressure during the annealing process [10, 11, 12]. The effect of oxygen content variation has a different nature with respect to cation doping. Doping cannot only be considered as a hole or electron source, but it can also create crystallographic defects in the perovskite lattice [13]. Engineering the oxygen or oxygen vacancies in the surface, film bulk or in the substrate interface region in manganites, can help us to obtain the optimal correlated behaviour and properties, which are appropriate for various technological applications.

We chose $Gd_{0.1}Ca_{0.9}MnO_3$ (GCMO) system for investigation of the effect of oxygen vacancy (V_O) or oxygen vacancy complex (V_O-$V_{A,B}$) concentrations on the structural, magnetic and transport properties. Our previous paper indicated that this system shows ferromagnetic-paramagnetic transition near 110 K and high electrical conductivity in a form of bulk material or thin film. The reported colossal magnetoresitivity properties [14] and memory effect on hysteresis loops below Curie temperature make this compound a good candidate in future memristor applications. All the interesting properties of the GCMO motivated us to explore the effect of oxygen content variation on structural, electrical and magnetic properties.

In the present paper, we report the effect of *in situ* oxygen and vacuum treatments on GCMO films with 0.9 Ca concentration grown by pulsed laser deposition. The structural, electrical and magnetic characterizations were done by the detailed x-ray diffraction (XRD), x-ray photoelectron spectroscopy (XPS) and SQUID magnetometry. We also investigate how the treatments affect on the defect types and vacancy concentration by positron annihilation spectroscopy (PAS).

2. Experimental methods

$Gd_{0.1}Ca_{0.9}MnO_3$ (GCMO) were deposited on Nb-doped $SrTiO_3$ (001)(STO) at 700°C with 1.75 torr oxygen pressure, by applying 1500 pulses of XeCl laser (λ = 308 nm) with the energy density of 1.3 J/cm^2. After the deposition, the films were kept at the atmospheric pressure of oxygen for 10 min at 700°C, before cooling them down to room temperature (pristine film). In order to investigate the effect of oxygen content variation on the GCMO film properties, the different *in situ* annealing treatments were done for the pristine film. For oxygen treatment, after deposition, the films were kept at the atmospheric pressure of oxygen for 60 min at 700°C and for vacuum treatment, the films were kept in a vacuum of 10^{-4} torr for 10 min at 600°C, before cooling them down to room temperature.

The XRD measurements were done using a Philips Empyrean diffractometer with 5-axis goniometer and PIXcel 3D detector. The lattice parameters and FWHM data were determined from $\theta-2\theta$ scans over $(00l)$, $(0hl)$ and (khl) peaks and 2-dimensional $\phi-2\theta$ scans of (224) peak. The x-ray photoelectron spectroscopy (XPS) spectra were obtained with Thermo Scientific Nexsa system. The spectra were collected using monochromated

Al Kα radiation and dual beam charge compensation. 50 eV pass energy was used to scan the core-level spectra. Vacancy like defects and their relative concentrations were determined by positron annihilation spectroscopy (PAS). The details of the experiments are given in the supplementary file of Ref. [15]. The temperature dependence of the magnetization was measured between temperatures of 10 and 400 K with a Quantum Design SQUID magnetometer in 50 mT external magnetic field with zero-field-cooled (ZFC) and the field-cooled (FC) cycles. The magnetic hysteresis curves were recorded in magnetic fields up to 5 T at temperatures of 10, 50, 100 and 400 K. The external field B was always oriented along the (110) direction of the films. The ZFC and FC curves of resistivity were measured in a standard four-probe method with the constant current of 0.5 μA at temperature range from 10 to 400 K and magnetoresistance measurements at 10, 50 and 300 K in the magnetic fields up to 9 T were made with the Quantum Design Physical Property Measurement System (PPMS).

3. Results and discussion

3.1. Effect of annealings on crystallographic properties

The overall scan of $\theta - 2\theta$ for GCMO films showed only (00l) and substrate peaks, no impurities were detected (Figs. 1a and 1b). The Gaussian function was fitted to obtain GCMO peak positions and the widths as the full width at half maxima (FWHM). The lattice parameters were determined with the Nelson-Riley method [16] from 2θ scan of (004), (024) and (224) peaks. The values are listed in Table 1. The FWHM values extracted from 2θ scans of (004) peak for oxygen treated film are slightly lower than those in the pristine film, indicating a more uniform c lattice parameter. However, the FWHM values in both 2θ and ϕ directions increase for vacuum treated sample. Thus, we can say that the vacuum treatment induces more variation in both the in-plane and out-of-plane directions (see Table 1). In comparison with the pristine film, the broad (224) peak in $\Delta\phi$ direction (Fig. 1b) and splitting of (002) GCMO peaks in 2θ scan (Fig. 1) could be signs of twin boundaries in the vacuum annealed film. The existence of twin boundaries in this sample, probably due to great number of oxygen vacancies and other defects, which increase the lattice distortion resulting in structural disorder has also been observed in other manganites [17]. The concentration of oxygen vacancies and other defects in this set of films will be discussed in the following section.

The unit cell volume, V, decreases slightly with oxygen annealing, while it increases with vacuum annealing in comparison with the pristine one. This change can be explained by the increased number of Mn^{3+} ions with ionic radius of 0.07 nm, when compared with the Mn^{4+} ions with ionic radius of 0.05 nm, leading to increased unit cell size. On the other hand, removing oxygen atoms with atomic radius of 0.12 from MnO_6 octahedron could lead to shrinkage of the unit cell. It seems that, in this set of GCMO films, the former explanation dominates and the vacuum treated sample with greater number of Mn^{3+} ions has larger unit cell, whereas the oxygen treated sample

has smaller unit cell, when compared with the pristine sample.

Table 1. Lattice parameters, lattice mismatch between the GCMO film and substrate in the in-plane direction, cell volume, 2θ peak width from (004) peak and ϕ peak width from (224) calculated from the room temperature XRD data. The thickness (D) and the roughness (r) of the surface and interface regions of all the films are extracted from XRR measurements implemented at room temperature. D_{inter} and r_{inter} stand for thickness and roughness of the interface, respectively. D_{surf} and r_{surf} are the thicknesses and roughnesses of the surface layer.

Films	a (Å)	b (Å)	c (Å)	V_{cell} (%)	FWHM $\Delta\theta(^\circ)$	FWHM $\Delta\phi(^\circ)$
Pristine	5.30	5.28	7.45	208.65	0.26	2.16
O_2-treated	5.30	5.27	7.44	208.51	0.23	2.18
Vacuum-treated	5.41	5.29	7.48	214.01	0.46	7.18
Films	D (nm)	D_{inter} (nm)	r_{inter} (nm)	D_{surf} (nm)	r_{surf} (nm)	
Pristine	89	5	0.6	1	0.5	
O_2-treated	90	4	1.4	2	0.6	
Vacuum-treated	88	11	3.8	3	0.6	

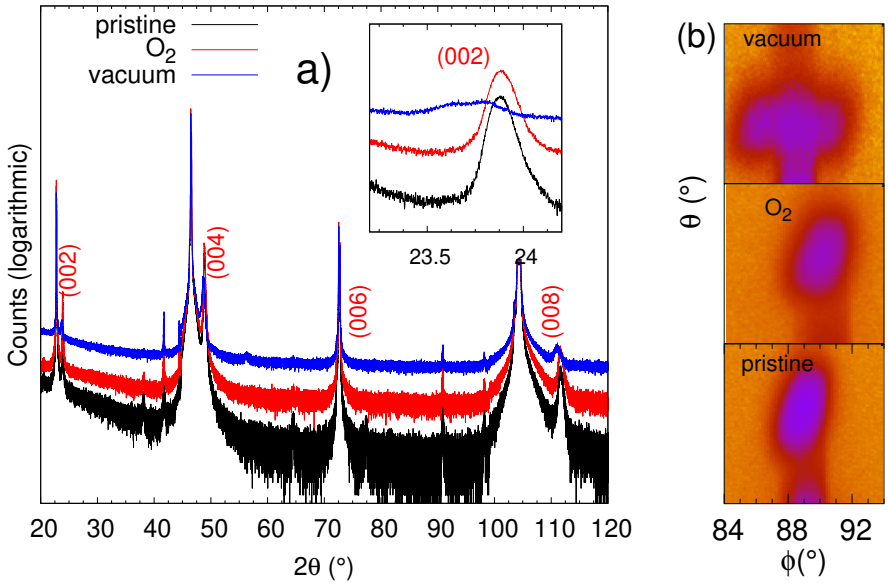

Figure 1. (a) The room temperature XRD patterns of GCMO films grown on STO substrate with different annealing treatments measured in (00l) direction. The inset exhibits the closer view of (002) peaks to show the splitting of the peak for vacuum annealed sample. The curves are shifted for clarity. (b) 2D 2θ-ϕ scan of (224) peak for all the films.

The lattice parameters in both in-plane and out-of-plane directions increase in the vacuum annealed sample in comparison with those of pristine one. This change is most pronounced in the a direction. In addition, introducing more oxygen vacancies in the GCMO lattice decreases the symmetry of the structure and turns the tetragonal pristine film to the orthorhombic [17, 18, 19]. The orthorhombic lattice relaxes by forming twins,

as can be seen in the (224) scans (see Fig 1b) and large $\Delta\Phi$ (Table 1) for this sample. This suggests that the oxygen vacancies form chains in the *a*-direction, similarly as observed for other perovskites [20, 21].

The thickness of the film, interface and surface layer, as well as roughness of the interface and surface of all the films were determined from the x-ray reflectivity measurements, where the fitting is made by using the GenX software [22] (Table 1). The effect of vacuum and oxygen annealings on thickness is insignificant and the thickness for all the films is around 90 nm. However, the thickness of the surface layer increases with oxygen and vacuum treatments, but the roughness of this layer does not change significantly (see Table 1). From previous literature, introducing/removing oxygen vacancies in perovskites' lattice resulting in thicker/thinner and rougher/smoother surface [23, 24]. In this case, it seems that even though upon oxygen annealing, the oxygen ions can fill the oxygen vacancies in the GCMO lattice, the film surface is also oxidized. Thus, the surface roughness increases. In order to confirm this the surface roughness of the pristine and annealed samples was measured by atomic force microscopy. The measurements showed that the roughness is almost the same for all the films, but the oxygen treated sample contains higher density of the nanosized particles on the surface. The oxygen treatment can increase the collisions among the evaporated atoms reducing the kinetic energy, thus lowering surface diffusion of the adatoms, which again favours the particle growth on the surface [25].

The thickness of the interface layer decreases slightly with oxygen treatment and the layer is much rougher than that of the pristine one. The roughness increases from 0.6 nm for pristine sample to 1.4 nm for oxygen annealed film. This can be explained by reoxidization of the substrate surface in the oxygen annealing process. As shown in Ref. [26], under typical conditions for perovskite film growth, the STO substrate exhibits Ti clustering and TiO_2 double layer on the surface, which results in rougher interface. Also, the vacuum treatment increased the thickness and roughness of the both interface and surface regions in comparison with the pristine sample, indicating more oxygen vacancies in both regions. The details of the oxygen vacancy and open volume defect concentrations will be discussed in the section of positron annihilation spectroscopy.

3.2. Electronic structure

In order to evaluate the oxidation states of the constituent elements, especially Mn present in the GCMO samples, XPS measurements were performed for all the films (see Fig. 2). All binding energies of the samples were calibrated by C 1s binding energy to compensate the surface charging effect. The full survey scans of pristine and annealed films confirm the existence of Gd, Ca, Mn, O and C on the surface of the films. The XPS spectrum of Mn 2p shows two peaks around 642 and 652 eV of binding energy, corresponding to Mn 2p3/2 and Mn 2p1/2, respectively. According to previous literature [27, 28, 29], a shoulder located at high energy side and the broadness of the peaks of Mn 2p3/2 and Mn2p1/2 can be contributed to the mixed valence state of Mn

ions. The Mn 2p peaks in Fig. 2a shows a clear shift (0.96 eV) toward lower binding energy side for vacuum treated film and a small shift (0.14 eV) to higher energy side of binding energy for oxygen treated film, when compared with the pristine sample. This can be due to increase of the number of Mn^{3+}/Mn^{4+} ions with vacuum/oxygen treatments. To confirm the change of Mn^{3+}/Mn^{4+} ratio with the vacuum and oxygen annealings, the Mn 3s core level spectra have been measured (Fig. 2b). The spectrum is split into two peaks due to the coupling of non-ionized 3s electron with 3d valence-band electrons [30]. The magnitude of the peak splitting indicates the oxidation state of Mn, meaning that ΔE for MnO (Mn^{2+}) is 6.0 eV, for Mn_2O_3 (Mn^{3+}) 5.3 eV and for MnO_2 (Mn^{4+}) 4.7 eV. In our samples, ΔE is 4.81 eV for the pristine one, indicating mixture of Mn^{3+} and Mn^{4+} valences in the sample. By vacuum annealing, this value increases to 5.1 eV, while it decreases to 4.6 eV in oxygen annealed film. Thus, the larger splitting indicates the greater number of Mn^{3+} ions in the vacuum treated sample. Similarly, the opposite change, slightly decreased in ΔE, can be attributed to the greater number of Mn^{4+} ions in the oxygen annealed sample in comparison with the pristine one.

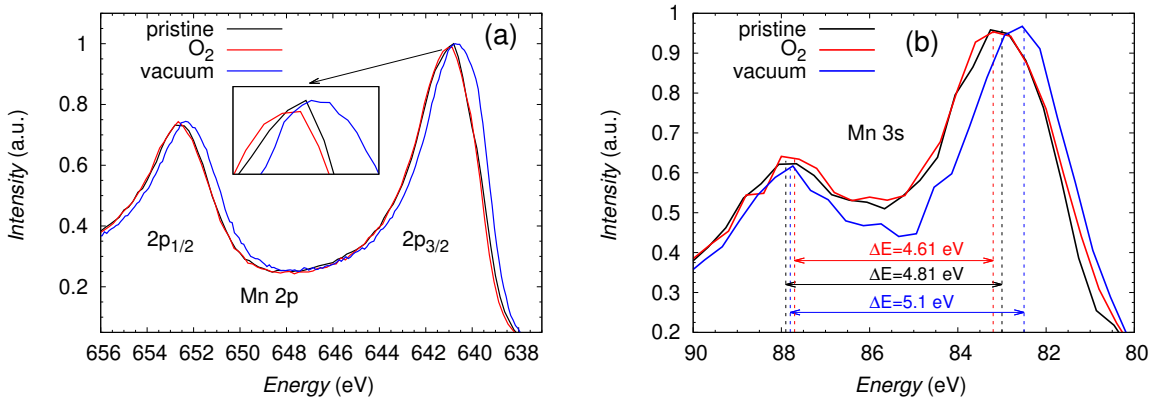

Figure 2. (a) The Mn 2p core level XPS spectra of pristine, O_2-treated and vacuum-treated GCMO films. The main panel displays the peaks at binding energy around 642 eV. The inset shows closer view of Mn $2p_{3/2}$ peak in order to reveal the detailed differences of Mn valencies. (b) The Mn 3s core level XPS spectra of the all films to show the magnitude of the splitting between 3s and 3d valence-band electrons of Mn ions.

3.3. Role of oxygen vacancies

Positron annihilation spectroscopy has been used to study the types of the defects in GCMO films. Positrons enable probing of open volumes in crystals, e.g., dislocations, vacancies and their agglomerations, as well as larger voids. Positrons are attracted to the empty spaces within the crystal with reduced Coulomb repulsive forces due to missing nuclei. There, the positron lifetime is increased and annihilation energy distribution is sharpened because of totally reduced electron density and larger probability of annihilation with valence electrons. This is evidenced by an increase of the annihilation

specific S-parameter, which scales with the defect density. The S-parameter represents a fraction of positron annihilated low momentum valence electrons normalized by the total number of events. The $S - E_{\mathrm{p}}$ curve, which illustrates the depth distribution of S, hence changes with defect concentration across film thickness.

The $S - E_{\mathrm{p}}$ curves for pristine, as well as for oxygen and vacuum annealed films are shown in Fig. 3. The relationship between S and E_p was analysed by using VEPFIT software providing as an output the so-called positron diffusion length L_+, a parameter inversely proportional to defect concentration [31]. The application of the software for the multilayer structures is described elsewhere [32]. Except for the substrate, two-layer model including the subsurface layer (GCMO film) and the interface layer should be considered.

The extracted diffusion length (L_+) for all the films is smaller than that for defect free materials with $l = 150 - 200$ nm [33, 34, 35]. Thus, the diffusion of positrons is suppressed by the trapping or scattering of defects in the GCMO films. In the film region, which according to the fit ranges down to at least 63 nm, the vacuum annealed sample has slightly larger S value and shorter diffusion length ($\sim$ 11 nm) compared with the oxygen treated sample. On the other hand, the latter one has the smaller S value and longer diffusion length ($\sim$18 nm) when compared with that of pristine one (see Table 2). The increase of L_+ in the film region for the oxygen treated sample can be attributed to lower defect density, e.g., lower concentration of oxygen vacancies and their complexes with the vacant sites of other elements.

In the interface region, the effect of vacuum treatment on vacancy concentration is more significant. The L_+ value decreases from 0.6 nm for pristine film to 0.1 nm for vacuum treated film, indicating the introduction of more vacancies in this region by vacuum annealing. As published earlier [36, 33, 32], when some complex perovskites epitaxially grown on STO in low pressure oxygen, the oxygen of the films can be automatically fed from the substrate. This can lead to the increase of oxygen vacancy concentration in the interface. Interestingly, the fit of beyond the interface region shows a large deviation, which suggests a necessity of additional layer representing emerging defects in the substrate due vacuum treatment. The oxygen annealed film has the same diffusion length in the interface as the pristine one, however, the thickness of the interface layer is significantly smaller. It seems that even though the oxygen annealing decreases the number of oxygen vacancies in the GCMO films, the reoxidazation of the substrate surface in the high pressure of oxygen can lead to increased density of vacancies in the interface. This is in agreement with the XRR data.

The positrons' lifetime spectrum measurement at room temperature was decomposed in three components for all the films. Based on free fitting with 3 or 4 lifetime components a reduced positron lifetime emerges, $\tau_0 \approx 50$ ps, which is a signature of partial bulk (interstitial) annihilation and annihilation in vacancy like defects. Besides bulk annihilation, two additional defect types have been found (τ_1 and τ_2), fitting with 4 lifetime components and fixing τ_0 to 50 ps for all the samples (Fig. 4). The derived lifetime values (τ_1 and τ_2) and their intensities are shown in Table 2. The first lifetime

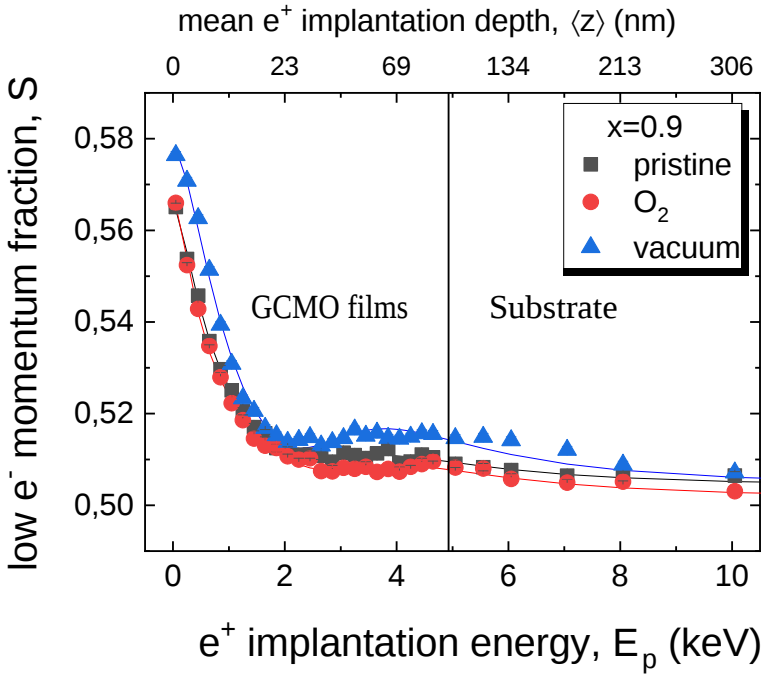

Figure 3. The S parameter (low electron momentum fraction) as a function of positron implantation energy E_p and mean positron implantation depth z_{mean}. The solid curves show the results of fitting under assumption that the density and overall thickness of the film layer and substrate are constant.

Table 2. The parameters calculated from the positron lifetime measurements for the pristine and annealed GCMO films. S_1, T_1 and L_1 are S parameter, thickness and diffusion length of the subsurface layer, respectively. For the interface layer, the S parameter, thickness and the diffusion length are shown by S_2, T_2 and L_2, respectively.

Sample	S_1	T_1 (nm)	L_1 (nm)	S_2	T_2 (nm)	L_2 (nm)
Pristine	0.502(4)	65(2)	10(4)	0.517(1)	21	0.6
O_2-annealed	0.496(6)	81(2)	17.7(5)	0.524(1)	9	0.5
Vacuum-annealed	0.505(3)	63(1)	11	0.531(9)	27	0.1
Sample	τ_1 (ps)	I_1 (%)	τ_2 (ps)	I_2 (%)		
Pristine	152–174	48–72	250–281	28–51		
O_2-annealed	116–141	29	∼223	∼73		
Vacuum-annealed	156–175	55–80	252–290	23–45		

τ_1 is about 175 ps with 72% intensity for the pristine film. The τ_1 value is close to the calculated value for lifetime positrons trapped by cation vacancies in B-site, V_B, (Mn or oxygen vacancies in the GCMO samples) [37]. The intensity increases to ∼80 % by vacuum treatment. This can be attributed to the formation of vacancy complex between V_B and oxygen vacancy (V_O) by removing oxygen from the film.

The derived second component of positron lifetime, τ_2, for pristine sample is approximately 280 ps. This value is slightly higher than the theoretical positron lifetime value for cation monovacancy in A-site (Gd or Ca in the GCMO cases) with 257–259 ps [37]. We can say that, τ_2 for the GCMO pristine film is probably a combination of cation

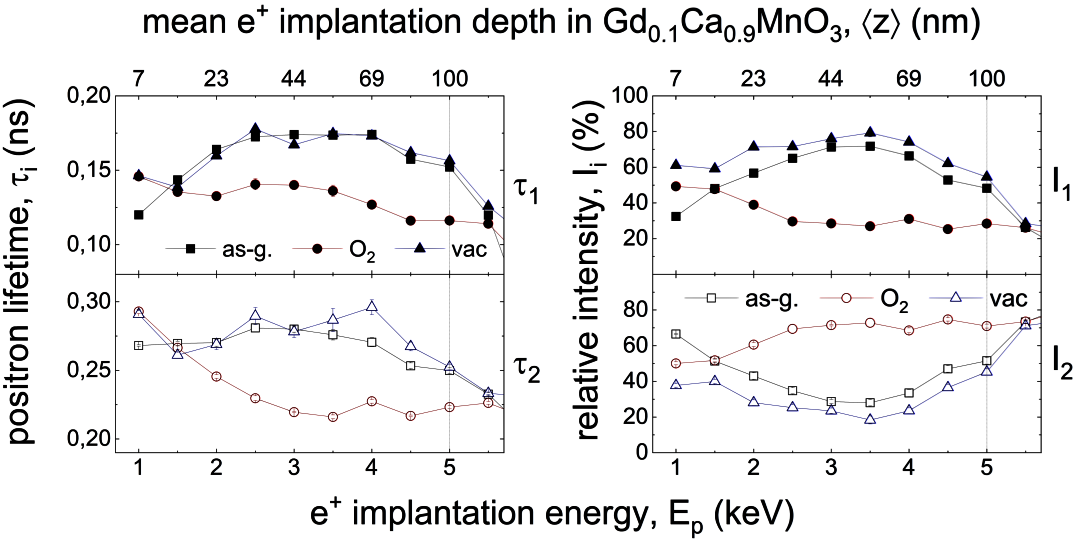

Figure 4. Positron lifetimes and their intensities as a function of E_p measured at room temperature.

vacancies at A-site with oxygen vacancies. Such complexes are often neutrally charged (Schottky defects), hence less attractive to positrons, which explains a slightly smaller intensity I_2 when compared with the pristine sample.

Both τ_1 and τ_2 decrease slightly to ∼140 ps and ∼220 ps, respectively, by oxygen annealing and this can be due to the smaller amount of oxygen vacancies. The intensity of the first component lifetime, τ_1, is below 30% for the oxygen treated film, which indicates the overall reduction of defect density, since the lifetime component close to the bulk value was detected. However, the A-site related lifetime vanishes, while the intensity increases, which can be explained by ionic migration to these particular crystal sites. It should be noted that the A-sites are large enough to accommodate all the possible elements in the system.

Thus, we can say that, the oxygen treatment likely refills single oxygen vacancies, but at the same time the $V_{\mathrm{Ti}} - -nV_{\mathrm{O}}$, where $n \geq 1$, can be generated due to ionic migration as can be seen in La:STO system [37]. This is confirmed by XRR data, which showed the rougher interface region when compared with the pristine sample.

3.4. Oxygen vacancy defined magnetic and magnetoresistive properties

The magnetization measurements as a function of temperature were performed with zero-field-cooled (ZFC) and field-cooled (FC) cycles in wide range of temperature, 10–400 K, for all the films. For pristine and oxygen treated films, the FC magnetization increases significantly as the temperature decreases and ZFC curves show a large peak below Curie temperature. This λ shape behaviour has also been observed in the electron doped region of other manganites [38, 39]. It is assumed that the peak in ZFC curves can

be attributed to cluster glass arising from competition between FM phase arrested in AFM phase (Fig. 5). However, the amplitude of this peak increases slightly for oxygen treated film when compared with the pristine sample. As schematically illustrated in Fig. 5b, the Mn ions magnetically interact each other through oxygen, which means that oxygen can share its electrons with the nearest Mn ions. When the Mn ions have different valence, the interaction is called as double exchange interaction that favours the FM configuration, while the interaction between Mn ions with the same valence is called as superexchange interaction, which favours the AFM configuration. It seems that the oxygen treatment could improve the double exchange interaction between Mn^{3+}–Mn^{4+} ions, thus increasing ferromagnetism.

To introduce more oxygen vacancies or vacancy complexes by vacuum treatment, the ferromagnetic part collapses (see Fig. 5a). This type of magnetic response to reduction of oxygen content has been reported for other manganites [17, 40]. In the vacuum-annealed film, the high concentration of V_O/V_{OB} in the GCMO lattice could destroy the double-exchange interaction between the Mn-O-Mn bonds and introduce a frustration into the magnetically coupled network that presumably leads to a spin-glass magnetic state. This is in agreement with the positron annihilation spectroscopy results, where V_O/V_{OB} concentration has been observed to increase/decrease with vacuum/oxygen treatments.

The Curie temperature (T_C) has been calculated from first derivative of magnetization vs. temperature (dM/dT), which is shown in the inset of Fig. 5a. The effect of oxygen annealing on T_C is insignificant, but T_C decreases for vacuum annealed sample (to ≈ 17 K). According to the previous publications, oxygen vacancies and defects in the crystalline structures of manganites as well as the tensile strain decrease the magnetic ordering temperature [41, 12, 42]. In this case, the positron annihilation spectroscopy results and XRD data show that the vacuum treated film have more oxygen vacancies or oxygen complex vacancies when compared with the pristine and oxygen annealed films. On the other hand, the unit cell in the in-plane direction is elongated in comparison with the pristine one. Therefore, these could lead to lowered T_C in the vacuum annealed film.

Table 3. The magnetic parameters of the films: T_C is the Curie temperature, M(5T) is the magnetization at 50 K and 5 T and H_C is the coercive field at 50 K. R(peak)/R(300) is the ratio of resistivity at metal-insulator transition temperature and room temperature.

Sample	M(5T) (10^8 A/m)	M(r) (10^8 A/m)	H_C (Oe)	T_C (K)	R(peak)/R(300)
Pristine	5	0.3	120	105	3.13
O_2-annealed	15	0.6	60	110	3.6
Vacuum-annealed	0.5	0.1	-	17	-

Fig. 5c–d show hysteresis loop curves for all the samples measured at 10 and 50 K. At 10 K, the pristine and the oxygen annealed samples show typical ferromagnetic

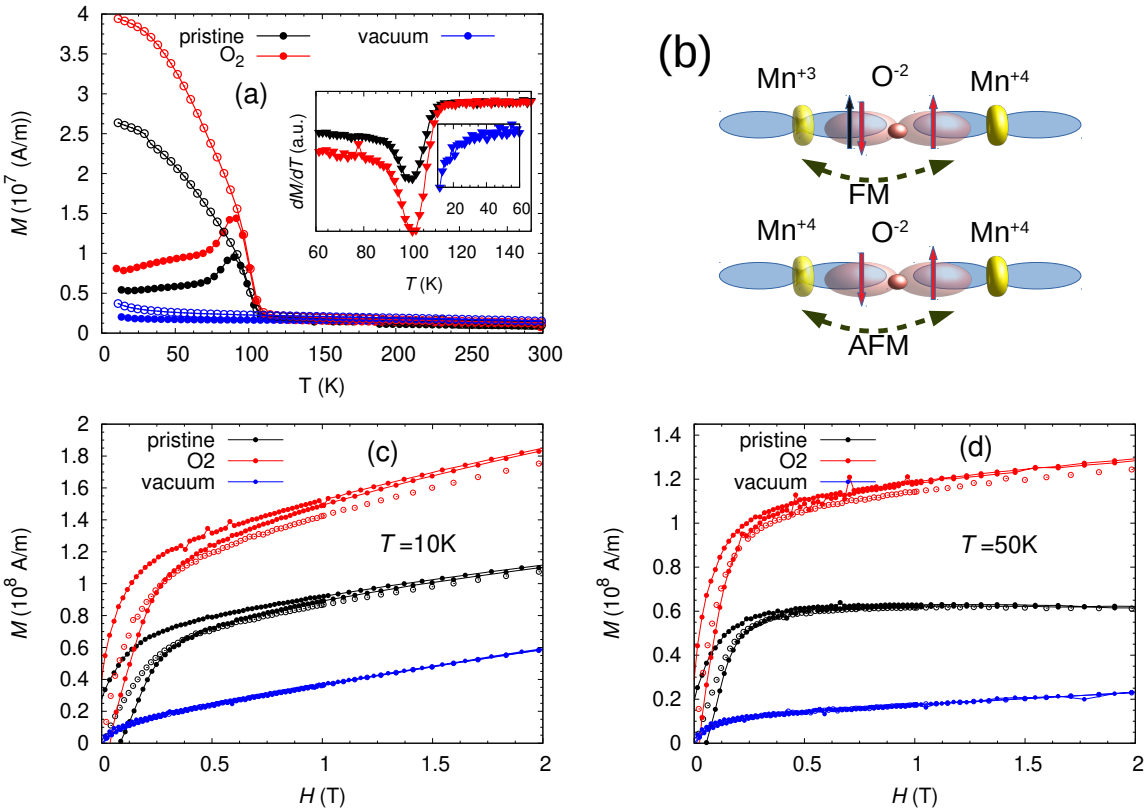

Figure 5. (a) The temperature dependences of ZFC and FC magnetization curves measured in 50 mT. ZFC curves are shown with filled symbols and FC curves with open symbols. The inset shows the temperature dependence of the first derivative dM/dT of the FC magnetization, where the peak position corresponds to T_C. (b) Schematic illustration of the interaction of Mn through oxygen in double exchange and superexchange interactions. (c) and (d) Part of the magnetic hysteresis loops together with virgin curves for pristine and for oxygen and vacuum treated films measured at 10 and 50 K, respectively, indicating the memory effect in the pristine and oxygen annealed films. The hysteresis loops are given with filled symbols and the virgin curves with open circles.

hysteresis loops. The magnetization increases rapidly in low magnetic field but it does not saturate below magnetic field of 5 T. This is due to AFM ordering of Mn^{3+}–Mn^{3+} and Mn^{4+}–Mn^{4+} pairs.

The magnitude of the magnetization at 5 T and the remanent magnetization (M_r) for oxygen treated film are higher than those of pristine one (see Table 3). The difference can be explained by increasing improvement of DE mechanism in the oxygen treated sample. Furthermore, as reported previously [14, 43], the pristine film displays the signature of the training effect above $H = 50$ mT, which means that by applying the external magnetic field from +5 to -5 T and back to +5 T, the magnetization retraces a different path from that of virgin curves. This spin memory effect is also observed in the oxygen treated film, being more significant with lower threshold field, 20 mT, in comparison with pristine one. The decrease of threshold field for spin memory effect

can be attributed to the increase of FM phase volume in the oxygen treated film.

At 50 K, the magnetization is saturated at 60 mT for pristine sample, however, the magnetization increases linearly by external magnetic field for oxygen treated sample (Fig. 6). It seems that the oxygen treatment not only makes the DE interaction strong but it also improves the superexchange interaction between Mn^{3+}–Mn^{3+} and Mn^{4+}–Mn^{4+} ions. Thus, the linear increase of magnetization vs. applied magnetic filed can be attributed to the stronger AFM-FM coupling for oxygen annealed film when compared with the pristine sample. As can be seen from data in Table 3, H_c for pristine sample is greater than that of oxygen treated one. As shown in other publications [44], greater number of oxygen vacancies result in larger coercive field, due to the magnetic domain wall pinning by oxygen vacancies. The vacuum treated film exhibits a typical spin glass loop, which can also be confirmed by $M(T)$ measurements.

The temperature dependence of resistance, $R(T)$, of GCMO films was measured without (filled symbol) and with (open circle) applied magnetic field. The pristine film shows insulating-metal transition around 100 K (Fig. 6), which could be attributed to the ferromagnetic cluster glass phase in this sample. Similar $R(T)$ curve with larger magnitude of resistivity in ZFC curve is observed for the oxygen annealed film. Both resistivity and resistivity ratio $R(\text{peak})/R(300)$ increase slightly by oxygen treatment (Table 3). This result was observed in multiple films with different histories. Interestingly, both the magnetic and PAS results would predict lower resistivity due to the increase of the FM phase volume and decrease of the amount of oxygen-manganese complex vacancies. On the other hand, the PAS results (Fig. 4b) show larger amount of Gd vacancies in oxygen annealed film and, based on XRR and AFM results, the sample has thicker dead layer at the surface with greater number of nanoscale particles when compared with the pristine film. It is suggested that the surface acts as an insulating barrier due to the breakage of crystal symmetry of the film, resulting in weakening of electron hopping in the lattice. These could explain the increased resistivity. For deeper understanding of the results, the density functional theory (DFT) calculations are required but they are out of the scope of this paper. The ZFC and FC curves bifurcate above the metal-insulator transition. The bifurcation is larger in the oxygen treated sample when compared with the pristine one, indicating stronger memory effect, which is in agreement with $M(H)$ measurements.

The magnetoresistance property (CMR), extracted from $R(H)$ were measured at 10 and 50 K for both pristine and oxygen samples. As can be seen from Fig. 6b, the resistivity decreases while the magnetic field increases (path(1)), meaning that the transition occurs from AFM-insulating (AFMI) state to FM-metallic (FMM) state. When the field is reversed, the resistivity changes in different path (2), and the films show smaller zero field resistance when compared with the virgin curve. This can be attributed to the partial recovery of the films to the original AFMI phase, as the magnetic field is reversed. This behaviour was reported also in previous publication [45, 46]. As temperature increases, the difference between the virgin curve and the subsequent cycles of $R(H)$ curves decreases (see Fig. 6c). This can be due to the thermal energy, which

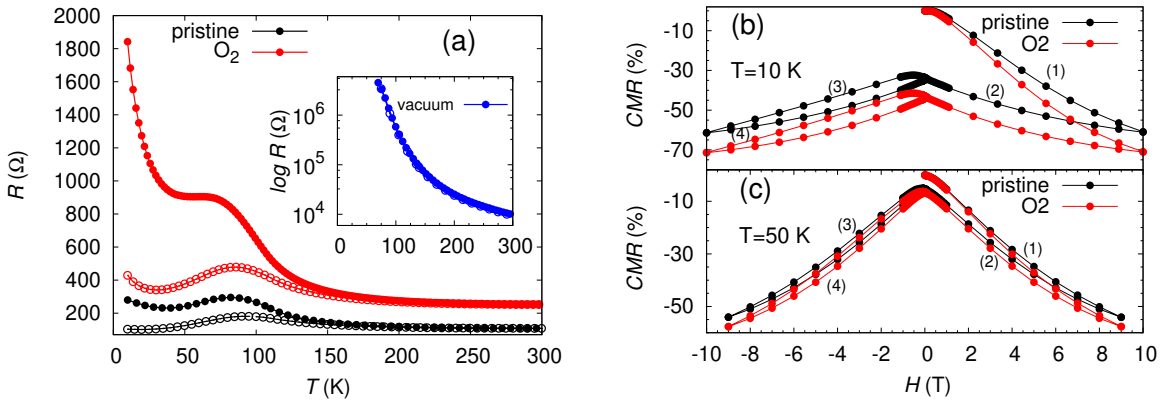

Figure 6. (a) Temperature dependences of the resistivity measured in 0 T (dots) and 9 T (open circles) fields for pristine as well as for oxygen and vacuum (inset) treated samples. (b) and (c) show the magnetic field dependence of the resistivity for pristine and oxygen annealed films measured at 10 and 50 K, respectively.

competes with the energy barriers between the FMM and AFMI phases, resulting in weakened FMM phase. The irreversible resistivity change with magnetic field is more significant in the oxygen annealed film when compared with the pristine film, indicating larger non-volatile CMR property in this sample. As shown in the schematic illustration of Fig. 7, FM phase volume could increase/decrease by introducing/removing oxygen ions in the film lattice, which again leads to improved/destroyed negative CMR property in the GCMO films.

4. Conclusion

The influence of oxygen content on low bandwidth manganite $Gd_{0.1}Ca_{0.9}MnO_3$ (GCMO) thin films was explored. Vacuum annealing turned the ferromagnetic-metallic GCMO film into the non-magnetic insulator, which was attributed to increase the content of Mn^{3+} ions, as observed from x-ray photoelectron spectroscopy (XPS) measurements and, on the other hand, the greater number of grain boundaries. In addition, the vacuum treatment decreased the Curie temperature T_C down to 17 K from the 105 K of the pristine one. The results were explained by a model suggested by the positron annihilation studies, where the number of oxygen vacancies and oxygen vacancy complexes in the A and B sites increases in both subsurface and interface regions.

In contrast to these results, the structural and magnetic measurements revealed that the ferromagnetic and magnetoresistance properties were modified below T_C by oxygen treatment, which can be explained by the double exchange mechanism. Furthermore, the spin memory effect was more significant and occurred at lower magnetic fields in oxygen annealed film when compared with the pristine film. However, the oxygen treated sample showed the larger magnitude of resistivity when compared with the pristine sample. These results were in good agreement with the positron annihilation results,

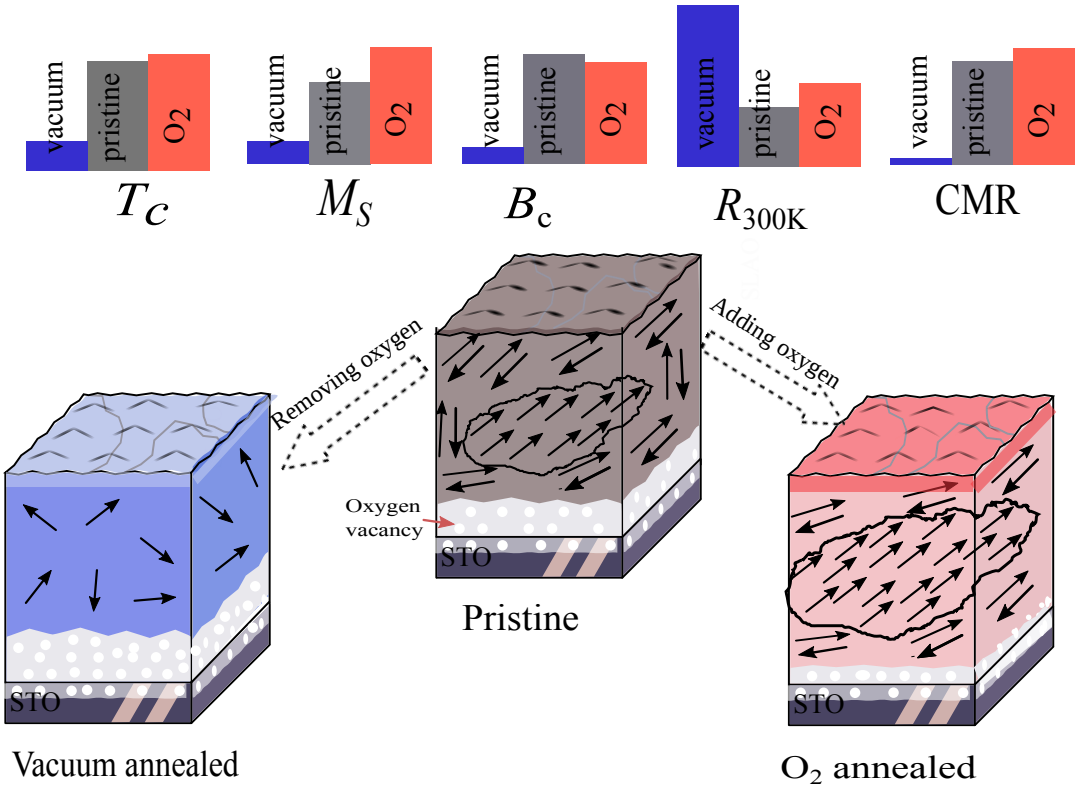

Figure 7. The schematic illustration how the oxygen and vacuum treatments affect the GCMO film. The arrows display the magnetic moments of the Mn ions and the domain structure. The oxygen treated film with thinner interface layer shows larger FM phase volume when compared with the pristine film. The vacuum treated film shows greater number of oxygen vacancies and oxygen vacancy complexes in the interface region, which leads to magnetic frustration in the GCMO lattice. In the panel on top, the collection how the treatments affect on the various magnetic and resistive properties are presented.

which demonstrated that the concentration of open volume defects was decreased by applying oxygen in the subsurface region of the film. The study suggested that one can manipulate magnetoresistance properties in the certain perovskite-like oxides by merely varying the oxygen content and hence design the modified oxides with great potential in the future memristor applications.

Acknowledgments

The authors wish to thank the Jenny and Antti Wihuri Foundation, Finland and the Academy of Finland (project no. 308285). AB also acknowledges the Väisälä foundation for financial support. Parts of this research were carried out at ELBE at the Helmholtz-Zentrum Dresden-Rossendorf e. V., a member of the Helmholtz Association. We would like to thank the facility staff for assistance. This work was partially supported by the Impulse-und Net-working fund of the Helmholtz Association (FKZ VH-VI-442

Memriox), and the Helmholtz Energy Materials Characterization Platform (03ET7015). The authors also are grateful to E. Hirschmann and A. G. Attallah for their technical assistance in the positron annihilation spectroscopy measurements.

References

[1] Martin C, Maignan A, Hervieu M and Raveau B 1999 *Phys. Rev. B* **60** 12191–12199
[2] Goto T, Kimura T, Lawes G, Ramirez A P and Tokura Y 2004 *Phys. Rev. Lett.* **92** 257201:1–4
[3] Hcini S, Boudard M, Zemni S and Oumezzine M 2014 *J. Ceram. Int.* **40** 16041–16050
[4] Liu C J, Bhaskar A and Yuan J J 2011 *Appl. Phys. Lett.* **98** 214101:1–3
[5] Schiffer P, Ramirez A P, Bao W and Cheong S W 1995 *Phys. Rev. Lett.* **75** 3336
[6] Beiranvand A, Tikkanen J, Huhtinen H and Paturi P 2017 *J. Alloy Compd.* **720** 126–130
[7] Prellier W, Lecoeur P and Mercey B 2001 *J. Phys. Cond. Mat.* **13** R915
[8] Zeng Z, Greenblatt M and Croft M 1999 *Phys. Rev. B* **59** 8784–8788
[9] Ahn K H, Lookman T and Bishop A R 2004 *Nature* **428** 401
[10] Klenov D O, Donner W, Foran B and Stemmer S 2003 *Appl. Phys. Lett.* **82** 3427–3429
[11] Majumdar S, Huhtinen H, Granroth S and Paturi P 2012 *J. Phys. Cond. Mat.* **24** 206002:1–8
[12] Trukhanov S V, Troyanchuk I O and Korshunov F P 2001 *J. Low Temp. Phys.* **27** 283–287
[13] Vergara J, Ortega-Hertogs R J, Madurga V, Sapina F, El-Fadli Z, Martínez E, Beltran A and Rao K V 1999 *Phys. Rev. B* **60** 1127
[14] Beiranvand A, Tikkanen J, Huhtinen H and Paturi P 2018 *J. Magn. Magn. Mater.* **469** 253–258
[15] Beiranvand A, Liedke M O, Haalisto C, ahteenlahti V L, Schulman A, Granroth S, Palonen H, Butterling M, Wagner A, Huhtinen H and Paturi P 2021 *J. Phys. Cond. Mat.* **33** 255803
[16] Nelson J B and Riley D P 1945 *Proc. Phys. Soc.* **57** 160–177
[17] Malavasi L, Mozzati M C, Ghigna P, Azzoni C B and Flor G 2003 *J. Phys. Chem. B* **107** 2500–2505
[18] Alessandri I, Bontempi E, Sangaletti L, Pagliara S, Malavasi L, Parmigiani F, Flor G and Depero L E 2004 *J. Phys. IV France* **118** 165–171
[19] Guo H, Wang J, He X, Yang Z, Zhang Q, Jin K, Ge C, Zhao R, Gu L, Feng Y, Zhou W, Li X, Wan Q, He M, Hong C, Guo Z, Wang C, Lu H, Ibrahim K, Meng S, Yang H and Yang G 2016 *Adv. Mater. Interfaces* **3** 1500753
[20] Juan D, Pruneda M and Ferrari V 2021 *J. Sci. Reports* **11** 6706
[21] Andersen N H, Lebech B and Poulsen H F 1990 *Physica C* **172** 31
[22] Björck M and Andersson G 2007 *J. Appl. Cryst.* **40** 1174–1178
[23] Li F, Zhan Y, Lee T H, Liu X, Chikamatsu A, Guo T, Lin H J, Huang J C A and Fahlman M 2011 *J. Phys. Chem. C* **115** 16947–16953
[24] Wang C, j Jin K, Gu L, b Lu H, m Li S and j Zhou W 2013 *Appl. Phys. Lett.* **102** 252401:1–4
[25] Ohring M 2002 *Materials Science of Thin Films (Second Edition)* (Academic Press)
[26] Herger R, Willmott P R, Bunk O, Schleputz C M, Patterson B D and Delley B 2007 *Phys. Rev. Lett.* **98** 076102
[27] Felhi H, Smari M, Bajorek A, Nouri K, Dhahri E and Bessais L 2019 *Prog. Nat. Sci.* **29** 198–209
[28] Gao J, Dai S Y and Li T K 2003 *Phys. Rev. B* **67** 153403:1–4
[29] Beyreuther E, Grafström S, Eng L M, Thiele C and Dörr K 2006 *Phys. Rev. B* **73** 155425:1–9
[30] Galakhov V R, M Demeter S B, Neumann M, Ovechkina N A, Kurmaev E Z, Lobachevskaya N I, Mukovskii Y M, Mitchell J and Ederer D L 2002 *Phys. Rev. B* **65** 13102
[31] van Veen A, Schut H, Clement M, de Nijs J M M, Kruseman A and Ijpma M R 1995 *Appl. Surf. Sci.* **85** 216–224
[32] Uedono A, Shimayama K, Kiyohara M, Chen Z Q and Yamabe K 2002 *J. Appl. Phys.* **92** 2697–2702
[33] Keeble D J, Wicklein S, Dittmann R, Ravelli L, Mackie R A and Egger W 2010 *Phys. Rev. Lett.* **105** 226102:1–4
[34] Mackie R A, Singh S, Laverock J, Dugdale S B and Keeble D J 2009 *Phys. Rev. B* **79** 014102:1–8

[35] Keeble D J, Singh S, Mackie A, Morozov M, McGuire S and Damjanovic D 2007 *Phys. Rev. B* **76** 144109:1–5
[36] Ghosh V J, Nielsen B and Friessnegg T 1999 *Phys. Rev. B* **61** 207–212
[37] Qin M, Gao F, Cizek J, Yang S, Fan X, Zhao L, Xu J, Dong G, Reece M and Yan H 2019 *Acta Mater.* **164** 76–89
[38] Krishna D, Lakshmi Y K, Sreedhar B and Reddy P V 2009 *J. Solid State Sci.* **11** 1312
[39] Boujelben W, Cheikh-Rouhou A, Pierre J and Joubert J 2001 *J. Alloys Compd.* **314** 15–21
[40] Liu B, Liu G, Feng H, Wang C, Yang H and Wang Y 2016 *Mater. Des.* **89** 715–720
[41] Millis A J, Darling T and Migliori A 1998 *J. Appl. Phys.* **83** 1588–1591
[42] Lee Y P and Park S Y 2004 *Appl. Phys. Lett.* **84** 777–779
[43] Schulman A, Palonen H, Lähteenlahti V, Beiranvand A, Huhtinen H and Paturi P 2020 *J. Phys. Cond. Mat.* **33** 035803
[44] Li B, Yang L, Tian J Z, Wang X P, Zhu H and Endo T 2011 *J. Appl. Phys.* **109** 073922:1–5
[45] Rawat R, Mukherjee K, Kumar K, Banerjee A and Chaddah P 2007 *J. Phys. Cond. Mat.* **19** 256211
[46] Wagh A A, Kumar P A, Bhat H and Elizabeth S 2009 *J. Phys. Cond. Mat.* **22** 026005